

Figure 1. Electron microscopy images of the porphyrin nanofiber bundles: a) TEM image; b) SEM image.

sized diameter) rods with a wide size distribution were obtained (see Fig. S1 in the Supporting Information). After formation, the morphology of the nanofiber bundles is not significantly altered by mild sonication.

The low-angle X-ray diffraction pattern of the porphyrin nanofiber bundles shown in Figure 1 is provided in Fig. S2a. The diffraction peaks at 8.96° and 4.10° may correspond to an ordered lamellar structure with an interlamellar spacing of 2.1 nm, approximately the same as the in-plane dimensions of the porphyrin tectons. High-resolution TEM images also show a minimum spacing of approximately 2.2 nm between the layers along the fiber axis (Fig. S2b).

The molar ratio of $[\text{SbOTPP}]^+$ to $[\text{H}_2\text{TPPS}_4]^{4-}$ in the nanofiber bundles was measured using elemental microanalysis (see the Supporting Information), UV-vis absorption spectroscopy (Fig. S3), and energy-dispersive X-ray (EDX) spectroscopy (Fig. S4). A ratio of 3.7:1 was obtained using elemental analysis, which is consistent with the values obtained from simulations of absorption spectra (3.5–4.0:1) and the less-accurate determinations using EDX spectroscopy. The measured ratio is close to the value of 4:1 that leads to neutralization of the charges of the ionic tectons without the participation of other ions in the solid.

The optical properties of the nanofiber bundles are quite different from those reported for porphyrin nanotubes.^[12] The UV-vis spectrum of the nanotubes shows intense red-shifted bands indicative of electronic coupling of the tectons in a J-aggregate structure. Similar bands are not seen in the UV-vis spectrum of a film of the nanofiber bundles cast on a quartz-glass substrate (Fig. 2b, inset). However, the Soret band in the nanofiber bundles (436 nm) is red-shifted compared to the monomeric porphyrins (Fig. S5), which might indicate the formation of J-aggregates without strong electronic

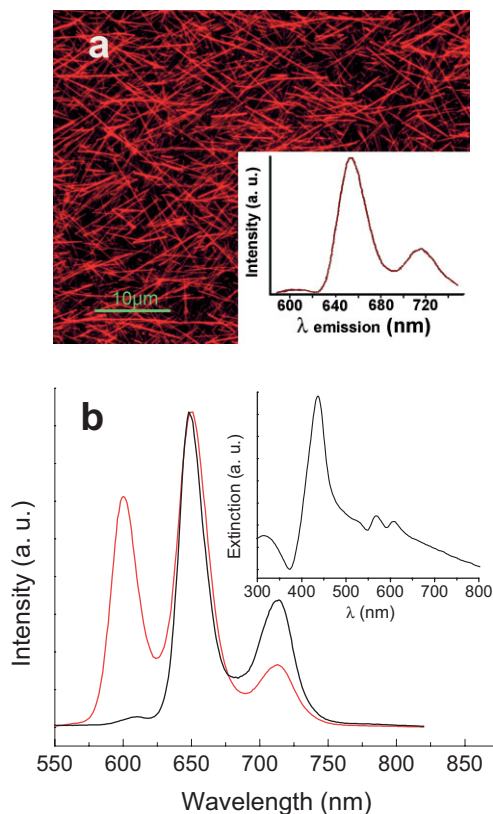


Figure 2. a) Confocal fluorescence microscopy image of the porphyrin nanofiber bundles. Inset in (a): representative emission spectrum from one spot on an individual fiber (excitation laser line: 488 nm) measured using a confocal microscope. b) Emission spectra of the nanofiber bundles dispersed in dichloromethane (black curve) or dissociated in ethanol (red curve) (excitation wavelength: 420 nm) measured using an Eclipse fluorimeter. Inset in (b): UV-vis spectrum of a film of porphyrin nanofiber bundles cast on a quartz-glass substrate.

coupling. Furthermore, the fluorescence of the porphyrins in the nanotubes is effectively quenched, whereas the porphyrin nanofiber bundles are highly fluorescent, emitting intense red light when excited with blue light, as shown by the confocal fluorescence image in Figure 2a.

The emission properties of the porphyrin nanofiber bundles were investigated in detail using a confocal microscope (Fig. 2a) and a conventional fluorimeter (Fig. 2b). The emission spectrum obtained from a single spot on an individual nanofiber bundle (Fig. 2a, inset) is consistent with the spectrum obtained from a suspension of nanofiber bundles in dichloromethane (Fig. 2b, black curve). Emission spectra of $[\text{SbOTPP}]^+$ and $[\text{H}_2\text{TPPS}_4]^{4-}$ (Fig. S6) indicate that the bands at 603 and 715 nm can be assigned exclusively to $[\text{SbOTPP}]^+$ and $[\text{H}_2\text{TPPS}_4]^{4-}$, respectively, while the band at 653 nm contains contributions from both porphyrins. Note that the 603 nm band is weaker than the 715 nm band in the spectrum of intact nanofiber bundles, but the relative intensities are reversed when the nanofiber bundles are dissociated into monomeric species in ethanol (Fig. 2b). This suggests that emission from $[\text{SbOTPP}]^+$ in the nanofiber bundles has been partially

quenched, possibly due to energy transfer from $[\text{SbOTPP}]^+$ to $[\text{H}_2\text{TPPS}_4]^{4-}$.

Despite these marked differences in optical and photophysical properties compared to the nanotubes,^[12] the nanofiber bundles still operate as photocatalysts. After the nanofiber bundles were exposed to visible light ($800 \text{ nmol cm}^{-2} \text{ s}^{-1}$) for 6 min in the presence of an aqueous solution of K_2PtCl_4 and ascorbic acid (as the electron donor), fairly uniform globular dendrites^[17] (ca. 50–70 nm in diameter) were observed on the surfaces of the bundles (Figs. 3a and S7a). The number and size of the dendrites can be controlled by varying the light-exposure time and/or the concentration of the platinum salt, consistent with the mechanism of photocatalytic seeding and autocatalytic growth discussed previously.^[17] For example, virtually continuous platinum coverage could be obtained with a

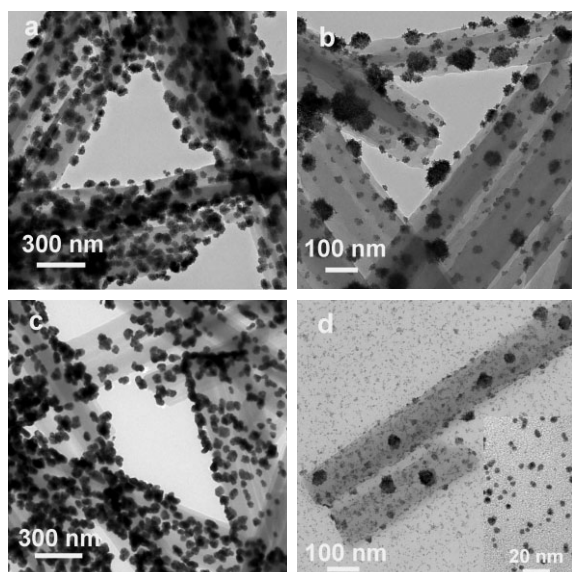


Figure 3. TEM images of porphyrin nanofiber bundles metallized with: a) platinum, b) gold, c) silver, and d) platinum–gold. Inset in (d): expanded view of the nanoparticles not attached to the nanofiber bundles. The durations of light exposure and solution compositions for the metallization reactions are: a) 6 min, 0.1 mM K_2PtCl_4 ; b) 8 min, 0.1 mM Au(I)-thiosulfate complex; c) 8 min, 1.0 mM Ag(I)-thiosulfate complex; and d) 8 min, 0.1 mM K_2PtCl_4 , 0.1 mM Au(I)-thiosulfate complex, all with 20 mM ascorbic acid.

tenfold increase in platinum concentration (Fig. S7b). In contrast, the reduction of colorless transparent solutions of Au(I)- or Ag(I)-thiosulfate complexes is predominantly photocatalytic rather than autocatalytic.^[13] Gold dendrites with a broad size distribution (10–100 nm) grow and remain bound to the surfaces of the nanofiber bundles (Figs. 3b and S8). Under high magnification, the gold dendrites are seen to have branches approximately 5 nm thick (Fig. S8). Metallization with a Ag(I)-thiosulfate complex produces reasonably uniform flattened particles (ca. 70 nm in diameter) on the surfaces of the nanofiber bundles (Figs. 3c and S9).

Intriguingly, when the photocatalytic/autocatalytic reaction is carried out in the presence of a solution containing equal concentrations of platinum and gold precursors, the main product is particles 2–5 nm in diameter (Fig. 3d). Some of the 2–5 nm particles are anchored on the nanofiber-bundle surfaces individually or as larger clusters, but most are dispersed on the TEM grid (Fig. 3d, inset). EDX spectroscopy studies show that the particles are predominantly gold (ca. 95 % gold and ca. 5 % platinum). One explanation for the unusual composition of these particles is that platinum seeds are easier to nucleate than gold seeds, but subsequent (photo)catalytic reduction of Au(I) onto the platinum seeds prevents their autocatalytic^[17] growth. Such differences in seeding rates, growth rates, and growth mechanisms (photocatalytic versus autocatalytic) most likely also explain the different size distributions seen for the platinum (Figs. 3a and S7a) and gold (Figs. 3b and S8) nanodendrites.

Additional studies show that a range of metalloporphyrins can be incorporated into the nanofiber bundles, which may allow tuning of their physicochemical properties. For example, nanofiber bundles with structures similar to those shown in Figure 1 are obtained when $[\text{SbOTPP}]^+$ is reacted with $[\text{MTPPS}_4]^{4-}$ (M = Cu, Ni, Ag, or Zn). All of these new nanomaterials are capable of photocatalytic metal reduction. For example, platinized nanofiber bundles produced from $[\text{SbOTPP}]^+$ and $[\text{CuTPPS}_4]^{4-}$ (Fig. S10) are similar to those obtained from $[\text{SbOTPP}]^+$ and $[\text{H}_2\text{TPPS}_4]^{4-}$ (Figs. 3a and S7a). Gilded nanostructures similar to those shown in Figure 3b are also obtained using nanofiber bundles prepared from $[\text{SbOTPP}]^+$ and $[\text{ZnTPPS}_4]^{4-}$ with a different electron donor (ethylenediamine tetra-acetic acid)^[18] (data not shown).

In summary, the synthesis of porphyrin-based nanostructures by ionic self-assembly has been extended to two-phase solution systems, allowing the use of a large library of water-insoluble porphyrin tectons and thus the synthesis of new porphyrin nanomaterials with a variety of functionalities. Using this phase-transfer ionic self-assembly method, we have prepared nanostructures composed of bundles of porphyrin nanofibers. These bundles show optical properties that are significantly different from those previously reported for porphyrin nanotubes,^[12] yet the fiber bundles possess similar reductive photocatalytic functionality.^[13] Their photoactivity is illustrated by their self-metallization reactions, which provide a facile means of preparing novel porphyrin–metal composite nanostructures that are expected to find important applications in electronics,^[2] photonics, catalysis,^[19–22] sensing,^[23] and solar hydrogen production. Attempts are underway to understand the differences and similarities in the photophysical and photochemical properties of the nanotubes and nanofiber bundles in terms of how the porphyrin tectons are arranged and interact inside these nanostructures.

Experimental

In a typical reaction, 9 mL of a 105 μM aqueous solution of $[\text{H}_2\text{TPPS}_4]^{4-}$ was added to 9 mL of a 315 μM dichloromethane solu-

tion of [SbOTPP]⁺ in a 20 mL glass vial. This biphasic mixture was first shaken vigorously for 2 min and then stirred vigorously with a magnetic stirrer bar for 1 h. The liquid/liquid interface re-established shortly after agitation was stopped, and strands of pink material immediately appeared in the organic phase. This material tended to float up to the interface but could be redispersed in the dichloromethane by gentle swirling. Samples for TEM and SEM imaging studies were prepared by pipetting 5–25 μ L of a suspension of the pink material onto standard holey carbon-coated copper TEM grids. The excess solvent was wicked away by a Kimwipe tissue placed underneath the grid.

For the self-metallization reactions, the nanofiber bundles were dried onto standard TEM grids, and the grids submerged in 1 mL of a solution of the metal precursor(s) (typically 0.1 or 1 mM) and ascorbic acid (typically 20 mM) in a 2 mL scintillation glass vial. The metallization reactions were performed at room temperature by irradiating the nanofibers with incandescent light ($800 \text{ nmol cm}^{-2} \text{ s}^{-1}$). The TEM grid was rinsed twice with deionized water prior to TEM imaging. Negligible amounts of gold or silver deposition were observed in control experiments without light or the porphyrin nanofiber bundles, confirming that these reduction reactions are predominantly photocatalytic.

TEM and EDX spectroscopy measurements were performed with a JEOL 2010 transmission electron microscope (200 keV). SEM imaging was carried out on a Hitachi S-5200 Nano Scanning Electron Microscope operating at 1 kV. The samples for TEM and SEM imaging were not subjected to any pretreatments such as heavy-metal staining or metal/carbon coating. X-ray diffraction patterns were recorded on a Siemens D500 diffractometer using nickel-filtered $\text{Cu K}\alpha$ radiation with $\lambda = 1.5418 \text{ \AA}$ in θ - 2θ scan mode. Fluorescence images were recorded using a Zeiss LSM510 META laser scanning microscope and a Zeiss fluorescence microscope with an Axioskop digital camera. UV-vis absorption spectra were obtained with a HP 8452A diode array spectrophotometer. The fluorescence measurements were carried out on a Varian Cary Eclipse fluorescence spectrometer.

Received: March 14, 2006
Final version: July 20, 2006

- [1] S. I. Stupp, *Chem. Rev.* **2005**, *105*, 1023.
- [2] A. P. H. J. Schenning, E. W. Meijer, *Chem. Commun.* **2005**, 3245.
- [3] T. Shimizu, M. Masuda, H. Minamikawa, *Chem. Rev.* **2005**, *105*, 1401.
- [4] P. V. Braun, P. Osenar, S. I. Stupp, *Nature* **1996**, *380*, 325.
- [5] B. H. Hong, S. C. Bae, C. W. Lee, S. Jeong, K. S. Kim, *Science* **2001**, *294*, 348.
- [6] K. M. Kadish, K. M. Smith, R. Guilard, *The Porphyrin Handbook*, Vol. 6, Academic, San Diego **2000**.
- [7] C. M. Drain, I. Goldberg, I. Sylvain, A. Falber, *Top. Curr. Chem.* **2005**, *245*, 55.
- [8] A. D. Schwab, D. E. Smith, C. S. Rich, E. R. Young, W. F. Smith, J. C. de Paula, *J. Phys. Chem. B* **2003**, *107*, 11 339.
- [9] J. H. Fuhrhop, U. Bindig, U. Siggel, *J. Am. Chem. Soc.* **1993**, *115*, 11 036.
- [10] C. F. J. Faul, M. Antonietti, *Adv. Mater.* **2003**, *15*, 673.
- [11] Y. Guan, S.-H. Yu, M. Antonietti, C. Bottcher, C. F. J. Faul, *Chem. Eur. J.* **2005**, *11*, 1305.
- [12] Z. Wang, C. J. Medforth, J. A. Shelnutt, *J. Am. Chem. Soc.* **2004**, *126*, 15 955.
- [13] Z. Wang, C. J. Medforth, J. A. Shelnutt, *J. Am. Chem. Soc.* **2004**, *126*, 16 720.
- [14] K. Kalyanasundaram, J. A. Shelnutt, M. Grätzel, *Inorg. Chem.* **1988**, *27*, 2820.
- [15] G. Knor, *Chem. Phys. Lett.* **2000**, *330*, 383.
- [16] G. Knor, A. Vogler, S. Roffia, F. Paolucci, V. Balzani, *Chem. Commun.* **1996**, 1643.
- [17] Y. Song, Y. Yang, C. J. Medforth, E. Pereira, A. K. Singh, H. Xu, Y. Jiang, C. J. Brinker, F. van Swol, J. A. Shelnutt, *J. Am. Chem. Soc.* **2004**, *126*, 635.
- [18] A. Moradpour, E. Amouyal, P. Keller, H. Kagan, *Nouv. J. Chim.* **1978**, *2*, 547.
- [19] B. Kraeutler, A. J. Bard, *J. Am. Chem. Soc.* **1978**, *100*, 4317.
- [20] Y. Jin, Y. Shen, S. Dong, *J. Phys. Chem. B* **2004**, *108*, 8142.
- [21] B. Yoon, C. M. Wai, *J. Am. Chem. Soc.* **2005**, *127*, 17 174.
- [22] D. Astruc, F. Lu, J. R. Aranzas, *Angew. Chem. Int. Ed.* **2005**, *44*, 7852.
- [23] B. J. Murray, J. T. Newberg, E. C. Walter, Q. Li, J. C. Hemminger, R. M. Penner, *Anal. Chem.* **2005**, *77*, 5205.